minerals

MDPI

Article

The Impact of Detrital Minerals on Reservoir Flow Zones in the Northeastern Bredasdorp Basin, South Africa, Using Core Data

Mimonitu Opuwari [1,*], Moses Okon Ubong [1], Simamkele Jamjam [1] and Moses Magoba [2]

[1] Department of Earth Sciences, Faculty of Natural Sciences, University of the Western Cape, Bellville, Cape Town 7530, South Africa
[2] Department of Geology, University of Forte Hare, Alice 5700, South Africa
* Correspondence: mopuwari@uwc.ac.za

Abstract: The present study uses core data to group reservoirs of a gas field in the Bredasdorp Basin offshore South Africa into flow zones. One hundred and sixty-eight core porosity and permeability data were used to establish reservoir zones from the flow zone indicator (FZI) and Winland's methods. Storage and flow capacities were determined from the stratigraphy-modified Lorenz plot (SMLP) method. The effects of the mineralogy on the flow zones were established from mineralogy composition analyses using quantitative X-ray diffraction (XRD) and Scanning Electron Microscopy (SEM). Results reveal five flow zones grouped as high, moderate, low, very low, and tight reservoir rocks. The high flow zone is the best reservoir quality rock and has porosity and permeability values ranging from 12 to 20% and 100 to 1000 mD. The high and moderate zones contribute more than 60% of each well's flow capacities. The moderate and low flow zone extends laterally to all the wells. The tight flow zone is an impervious rock and has the lowest rock quality with porosity and permeability values less than 8% and 1 mD, respectively. This zone contributes less than 1% to flow capacity. The impact of minerals on flow zones is evident in plagioclase and muscovite content increases. An accompanied decrease in quartz content is observed, which implies that low plagioclase content $\leq$4% and muscovite content of $\leq$1% corresponds to the low, moderate, and high flow zones, while plagioclase content of $\geq$4% and muscovite content of $\geq$1% belong to the tight flow zone. Consequently, the quantity of plagioclase and muscovite can be used as a proxy to identify better quality reservoir rocks. The diagenetic process that reduces the rock quality can be attributed to quartz overgrowth and the accumulation of mica flakes in the pore spaces. In contrast, the fracture in the high flow zone is the reservoir quality enhancing process. The flow zones are generally controlled by a combination of facies and diagenetic factors.

Keywords: flow zone; storage and flow capacities; minerals; Bredasdorp Basin

Citation: Opuwari, M.; Ubong, M.O.; Jamjam, S.; Magoba, M. The Impact of Detrital Minerals on Reservoir Flow Zones in the Northeastern Bredasdorp Basin, South Africa, Using Core Data. *Minerals* **2022**, *12*, 1009. https://doi.org/10.3390/min12081009

Academic Editor: Georgia Pe-Piper

Received: 23 July 2022
Accepted: 4 August 2022
Published: 12 August 2022

1. Introduction

Reservoir rock delineation in a heterogeneous formation is complicated and requires an accurate integration of petrophysical and petrography evaluation because each rock has its petrophysical, petrographical, mechanical and depositional characteristics [1–7]. Detailed reservoir characterization is possible by using petrophysical core data with a petrography study by dividing the reservoir into different zones based on similar hydraulic rock units or petrophysical rock types. The delineation of reservoirs into zones or units of hydraulic flow units has been studied and applied successfully by many authors [8–12]. To aid the classification of reservoir rocks based on the contribution of rock types, key terms such as Flow Unit (FU), Hydraulic Flow Unit (HFU) and Petrophysical Rock Type (PRT) within the reservoir have been defined [1,13]. To understand the storage and flow capacities of and the petrophysical behaviour of the FU, HFU and PRT within a reservoir, the Stratigraphy-Modified Lorenz Plot (SMLP) is one of the methods that has proven to be successfully applied by many authors in both carbonate and clastic reservoirs [14].

The impact of the depositional environment and diagenesis on reservoir quality is crucial because of the heterogeneity of sedimentary rocks, which also contributes to the variations of reservoir quality within a reservoir [15–20]. The quality of a reservoir is the primary factor that controls the prospectivity, especially during the exploration and production of hydrocarbon [21,22]. Due to the importance of reservoir quality in the assessment of the productivity of a reservoir, it is necessary to conduct an integrated core analysis, well log, and petrography studies to obtain the details of the composition of minerals that affect the reservoir quality. Consequently, the shallow marine sandstone reservoirs of wells MO7, MO8 and MO9 of a gas field in the northeastern Bredasdorp Basin, offshore of South Africa, have been studied with the help of conventional core data, sedimentology reports, well logs, and petrography data. To better understand the diagenetic impacts of the reservoir quality of the gas-producing zones, integrated petrographic analyses of X-ray diffraction (XRD), thin section and scanning electron microscopy (SEM) investigations, as well as core porosity and permeability measurements, have been studied.

Previous studies on gas-bearing reservoir flow units and zonation in the Bredasdorp Basin in South Africa [23–25] were conducted in the central, northwestern and the western parts of the Bredasdorp Basin. These previous studies on flow zonation in the Bredasdorp Basin identified various flow zones. In some cases, they also integrated XRD data and repeat test analysis to understand the lateral extents of the flow zones and the dominant mineral that controls flow zones. However, a gap exists because the works were not extended to the northwestern part of the Basin. Therefore, the present study aims to vigorously undertake integrated comprehensive petrophysical and petrographic reservoir zonation investigations to identify flow zones and correlate them with the identified zones in the other parts of the Basin. In addition, the study also attempts to understand the impacts of minerals on petrophysical reservoir flow zones. To achieve the objectives of this study, conventional core porosity and permeability data are integrated with sedimentology framework and mineralogy analyses that allows the delineation of the reservoir units into flow zones.

2. Overview of Geological Setting

The present study used three wells, MO7, MO8, and MO9, situated in the Bredasdorp Basin, offshore of the southern part of South Africa (Figure 1). The Bredasdorp basin sediments are predominantly derived from the processes of erosion and stripping of the shallow, deep and transitional marine environments of Cape Supergroup and Karoo Supergroups [26,27]. Consequently, the primary source of hydrocarbons in the basin is the deep marine mature shales deposited in the mid-Aptian. The synrift shelf and drift section of deep marine turbidite sandstone form the two major basinal reservoirs, while the drift shales of marine origin act as the primary seals.

The wells have been drilled to test for hydrocarbons at the primary target formed by a sequence of stacked transgressive and regressive shallow marine sandstones. The sandstone within the shallow marine sequence is interpreted as being deposited in a relatively high-energy, sand-dominated, tide- and wave-influenced environment [28]. Several authors have reported that the Bredasdorp Basin was formed in the Gondwana due to the movement of the South Atlantic along the Agulhas–Falkland Fracture Zone [20,26,29]. In addition, several authors have made significant contributions [25,27,30–34] to study sedimentology, sequence stratigraphy, petroleum systems, and the regional tectonic settings of the Bredasdorp Basin. However, to date, few published works have been published on the impacts of mineral composition on the variations of flow zonation in the Bredasdorp Basin, offshore of South Africa.

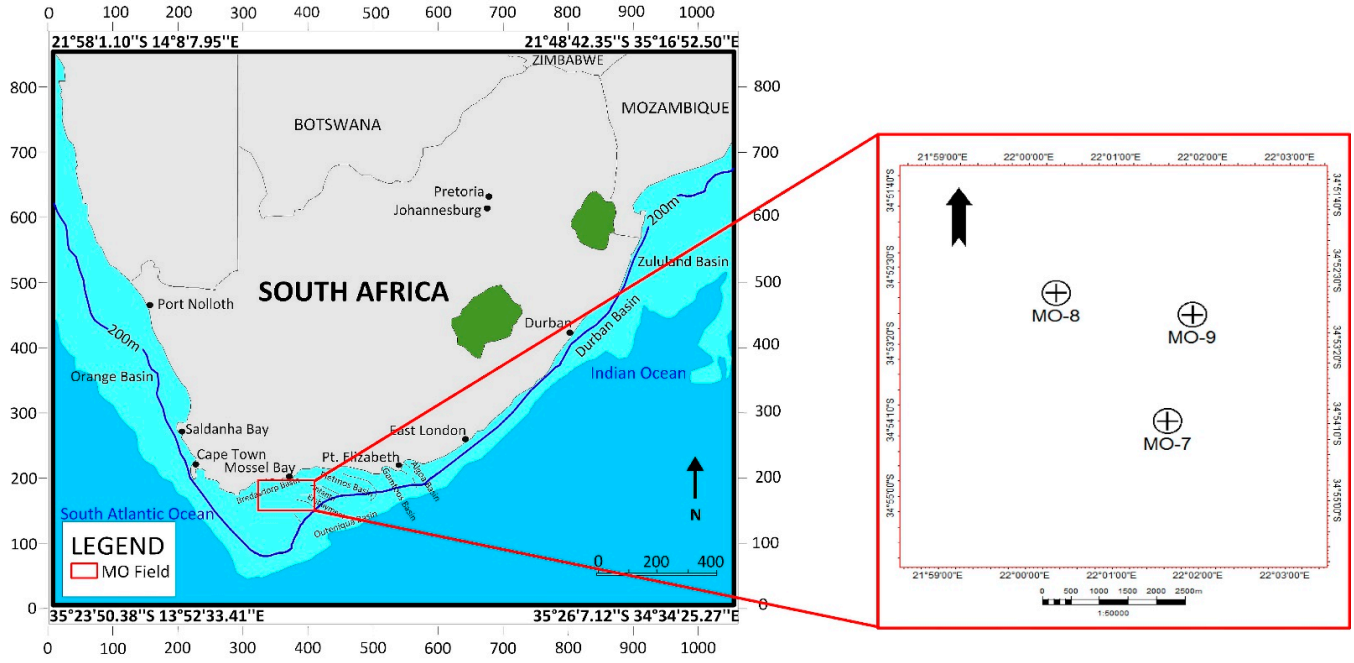

Figure 1. Maps showing the area of study offshore South Africa and the location of the wells.

3. Materials and Methods

The datasets, including gamma ray well log, core analysis (permeability and porosity), and sedimentology data (reports, SEM and XRD analyses), are available for the studied wells (MO7, MO8 and MO9) of the northeastern Bredasdorp Basin, offshore of South Africa. First, a database was created in Interactive Petrophysics (IP 4.7) software, and all the datasets were loaded. Then, the quality control of data was implemented. The well logs were used to identify the reservoir intervals, lithology and well log-core measurements shift. A total of 168 core plug samples of the wells were examined from the routine core analysis results. The analyses included porosity and permeability measurements using the Vinci Technology poroperm equipment measured at room condition. The well logs indicate that the logger's depth is 2.45 m deeper than the driller's depth over the cored interval for well MO9. Therefore, a well-core depth shift was performed. In the other wells (MO7 and MO8), a match between the logger's depth and the driller's depth was observed.

Thirty plug samples from well MO7, 70 from well MO8 and 68 from well MO9 were taken to determine the petrophysical properties used for the reservoir zonation. The process commenced with facies identification, followed by the analyses of two independent analytical methods (PRT from the Winland r35 and FZI) and (2) SMLP and then the integration of mineralogy analyses.

3.1. Facies Analysis

Core samples were visually examined and integrated with core description reports and gamma-ray logs provided by PASA, which was used to classify the core samples into distinct facies. The studied reservoir units were classified based on texture, grain sorting, log shapes/patterns and gamma-ray log values.

3.2. Flow Zone Identification Methods (Winland r35, FZI and SMLP)

To divide the reservoir into flow zones from core porosity and permeability, the [35] pore throat radius flow determination and the concept of flow zone Indicator (FZI) by [36] methods, successfully applied by other researchers [37–41], was applied to slice the reser-

voirs into flow zones accurately. The pore throat radius from core porosity and permeability was calculated from Winland's r35 method [35,42] as:

$$\text{Log r35} = 0.732 + 0.588 \log \text{K} - 0.864 \log \text{Ø} \quad (1)$$

where r is pore throat radius (μm), K is the permeability (mD) and Φ is the porosity (%).

We also adopted the method of [36] to assess the hydraulic flow zones, which utilizes the reservoir quality index (RQI), normalized porosity index (NPI) and flow zone indicator (FZI). In addition, to determine the contribution of storage and flow capacities of flow zones, the SMLP method of [43] was adopted. The SMLP is based on plotting the cumulative flow capacity against the cumulative storage capacity, and significant inflexion points indicate the point of departure from one flow unit or zone to another. The details on how to calculate the capacities are published by [1,39,44–47].

The SMLP method was implemented in the three wells (MO7, MO8 and MO9) to establish storage and flow capacities because the petrophysical rock type methods cannot establish each zone's storage and flow capacities.

3.3. Mineralogy Analyses

To assign the mineral composition in a flow zone, a representative of four samples collected for mineralogy analysis. Additionally, detailed mineral composition using the XRD technique was adopted to determine the percentages of different minerals and provide additional visual character details of the structure of the pore spaces. The black loading material preparation method was used for the four samples' XRD qualitative and quantitative XRD analysis. According to [48], the identification of minerals was based mainly on peak shapes and positions. For the quantitative analysis, amorphous phases, if present, were not considered during quantification. In addition, SEM was performed to provide information on pore types and clay mineral morphology and distribution and to collaborate the results with thin section and XRD measurements.

4. Results and Discussion

4.1. Facies

The reservoir sediments assessed are predominantly of shallow marine depositional environment. The lithology and sedimentary structures in the core intervals varied with depth and strongly correlated with log data. The cored intervals were classified into four facies by combining the visual inspection of the core, grain size distributions, and log data. The four facies identified are:

- Facies A: Moderately to well-sorted, medium-grained with conglomerate intervals developed;
- Facies B: Fine- to medium-grained sandstone, slightly glauconitic;
- Facies C: Fine- to medium-grained sandstone, poorly sorted, very glauconitic;
- Facies D: Siltstone, very fine-grained with claystone.

Well MO7 has facies B and facies C present, while well MO8 has facies A and B. All the facies are present in well MO9 (Figure 2). Facies A is classified to have the best reservoir quality, while facies B's reservoir quality is termed good. The reservoir quality of facies C is termed intermediate, while facies D is termed poor reservoir quality. Facie D is manifested at the top and bottom of wells MO7 and MO9, suggesting good seal rocks within both wells. The absence of facies D at the top of well MO3 may illustrate a poor reservoir seal.

4.2. Flow Zone Modelling

4.2.1. Winland r35

The results of the pore throat radius calculated from the Winland r35 pore throat radius methods are presented in Table 1 and Figure 2, respectively. The calculated average value of pore throat radius of an interval was used to represent flow zone designated as (PRTs) based on the criteria below:

Megaoporous rock (≥10 µm) = PRT1;
Macroporous rock, from 4.0 to 10 µm) = PRT2;
Mesoporous rock, from 2.0 to 4 µm = PRT3;
Microporous rock (from 1 to 2 µm) = PRT4;
Nanoporous rock (≤1 µm) = PRT5.

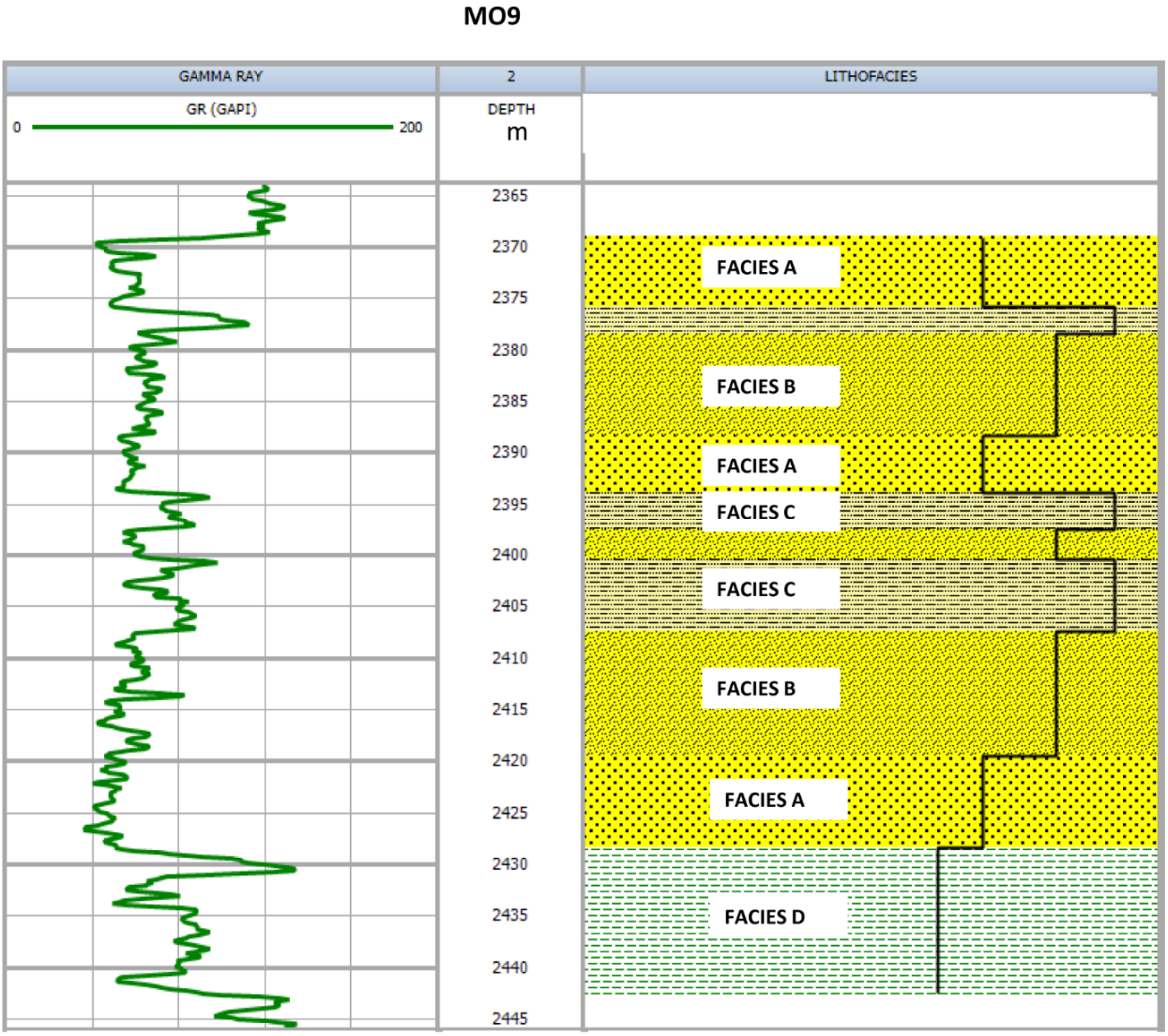

Figure 2. Well MO9 showing gamma ray log in track one and four different facies classified as facies A, B, C and D in track three.

Figure 3 presents five distinct PRTs (PRT1–5). It can be seen that the lower the value of r35 calculated (PRT1 and 2) represent smaller pore throats and lower permeability values. In contrast, the high r35 values (PRT4–5) resulted in higher pore throats and permeability. PRT3 is an intermediary rock type between the higher and lower pore throats. It was also observed from Figure 3 that, for porosity in the range of 12–21%, higher permeability values from 20 to 1000 mD indicate better reservoir qualities (PRT1 and 2). PRT1 is the best rock type, while PRT5 is the lowest rock type.

Table 1. Results of calculated petrophysical rock types and flow zone indicators used to classify rocks into different flow zones.

Well	Top Depth (m)	Bottom Depth (m)	Thickness (m)	Porosity %	Permeability mD	Zone	r35 (μm)	PRT/HFU	Rock Type	FZI (μm)	Ranking
				12–22	200–1000	High	≥10	1	Megaporous	≥6	Very Good
				10–12	20–200	Moderate	4–10	2	Macroporous	3–6	Good
				5–10	5–20	Low	2–4	3	Mesoporous	2–3	Fair
				5–10	1–5	Very Low	1–2	4	Microporous	1–2	Poor
				<5	<1.0	Tight	<1	5	Nanoporous	≤1	Impervious
MO7	2415.1	2418.0	2.9	6.0	2.1	Very Low	3.4	4	Microporous	2.2	Poor
	2418.0	2429.3	31.3	7.8	29.8	Moderate	8.3	2	Macroporous	4.9	Good
	2429.3	2435.7	6.4	5.9	10.8	Low	4.1	3	Mesoporous	2.3	Fair
	2435.7	2443.3	7.6	7.3	53.8	Moderate	10.1	4	Macroporous	5.8	Good
	2443.3	2446.6	3.1	4.9	0.5	Tight	1.2	5	Nanoporous	0.9	Impervious
MO8	2368.2	2380.1	11.9	13.7	237.0	High	15.2	1	Megaporous	8.1	Very Good
	2380.1	2396.0	15.9	12.2	65.0	Moderate	7.0	2	Macroporous	4.9	Good
	2396.0	2417.6	21.6	11.5	29.0	Moderate	5.0	2	Macroporous	3.2	Good
	2417.6	2436.8	19.2	11.7	42.0	Moderate	5.8	2	Macroporous	3.9	Good
	2436.8	2445.2	8.4	11.2	18.0	Low	3.3	3	Mesoporous	2.6	Fair
MO9	2369.2	2376.2	7.0	16.8	842.0	High	27.0	1	Megaporous	11.6	Very Good
	2376.2	2387.2	11.0	12.2	27.5	Low	4.3	3	Mesoporous	3.0	Poor
	2387.2	2393.3	6.1	15.3	300.0	High	14.0	1	Megaporous	6.8	Very Good
	2393.3	2419.3	26.0	12.8	43.0	Moderate	6.7	2	Macroporous	4.2	Good
	2419.3	2428.2	8.9	12.9	277.0	High	16.0	1	Megaporous	10.0	Very Good
	2428.2	2442.4	14.2	10.1	0.5	Tight	0.7	5	Nanoporous	0.8	Impervious

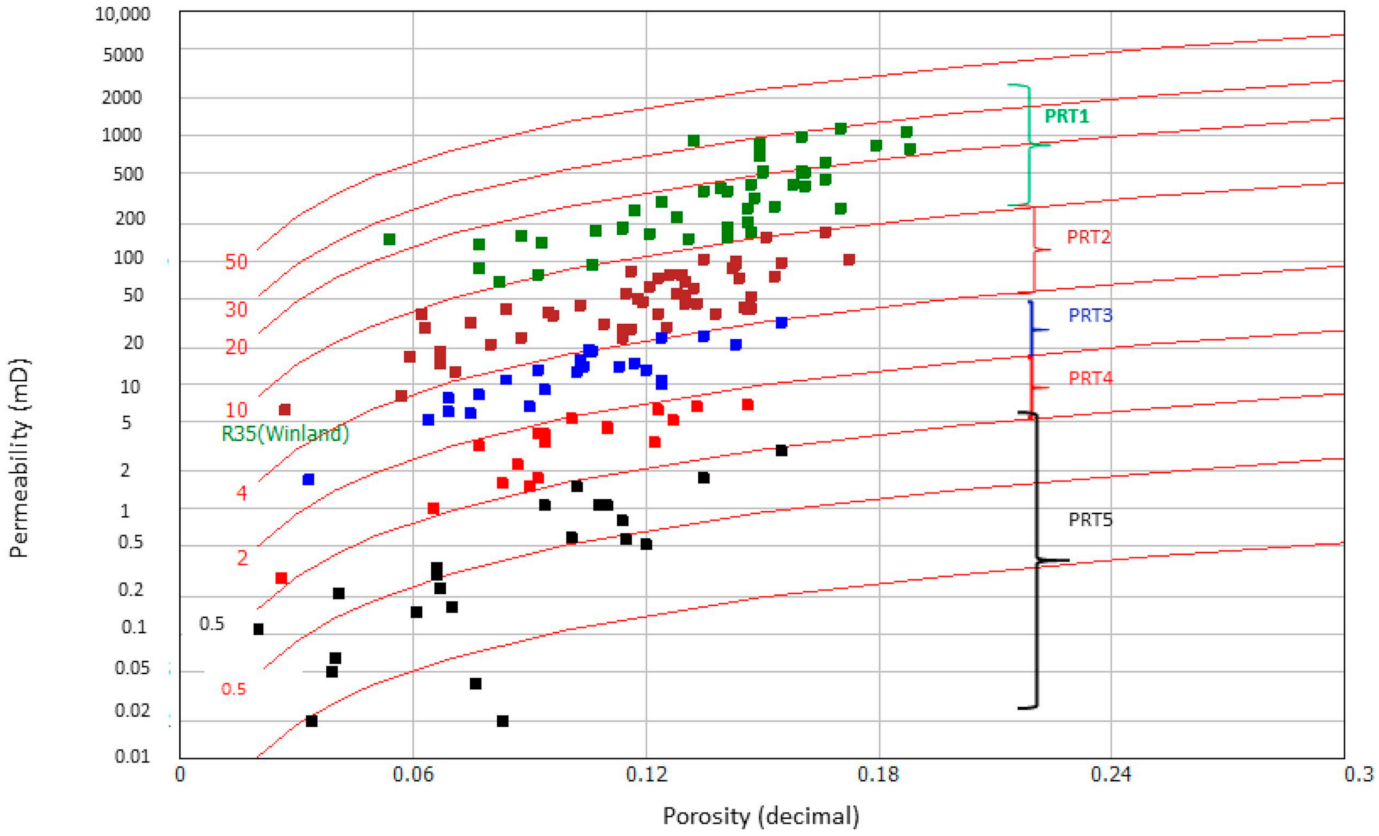

Figure 3. Calculated Windland r35 pore throat radius showing five different petrophysical rock types (PRT1-5) plotted on the standard Windland graph on permeability against porosity.

4.2.2. Flow Zone Indicator

The results of the computation of FZI for the studied wells using the modified classification criteria of [49] resulted in five distinct HFUs from 0.8 to 11.6 µm, as presented in Table 1. The criteria used for the classification of the flow zones are:

HFU1 = ≥6 µm;
HFU2 = 3–6 µm;
HFU3 = 2–3 µm;
HFU4 = 1–2 µm;
HFU5 = ≤1 µm.

From Table 1, we can deduce that HFU5 correlates to PRT5, which is the impervious rock type; HFU4 to PRT4, which is a poor rock type; HFU3 to PRT3, ranked as a fair rock type; HFU2 to PRT2, which is good reservoir rock; and HFU1 to PRT1, a very good reservoir rock.

The highest FZI value of 11.2 µm was recorded in well MO9 which has a thickness of 7.0 m, a porosity of 17.2% and an average permeability of 942 mD. The lowest FZI value of 0.8 µm was recorded in well MO9, with a thickness of 14.1 m, a porosity of 10% and permeability of 0.5 mD (Table 1). By visual observation, the RQI versus NPI plot on a log-log scale generally showed five distinguishable HFUs with some overlap (Figure 4a).

The permeability, porosity and FZI of each type of flow unit are presented in Figure 4b. Figure 4b illustrates a significant difference in the flow units' permeabilities, reflecting different fluid transmissibility. However, the porosity does not clearly distinguish between flow units except for HFU5, which generally displayed porosity values less than 12%. Therefore, for low permeability sandstone gas reservoirs, to which the Eastern Bredasdorp Basin belong, we propose that to differentiate between impervious rocks and reservoir rocks, a porosity cut-off value of 8% with a corresponding permeability of 1 mD be used to exclude impervious rocks from our reservoir rock units.

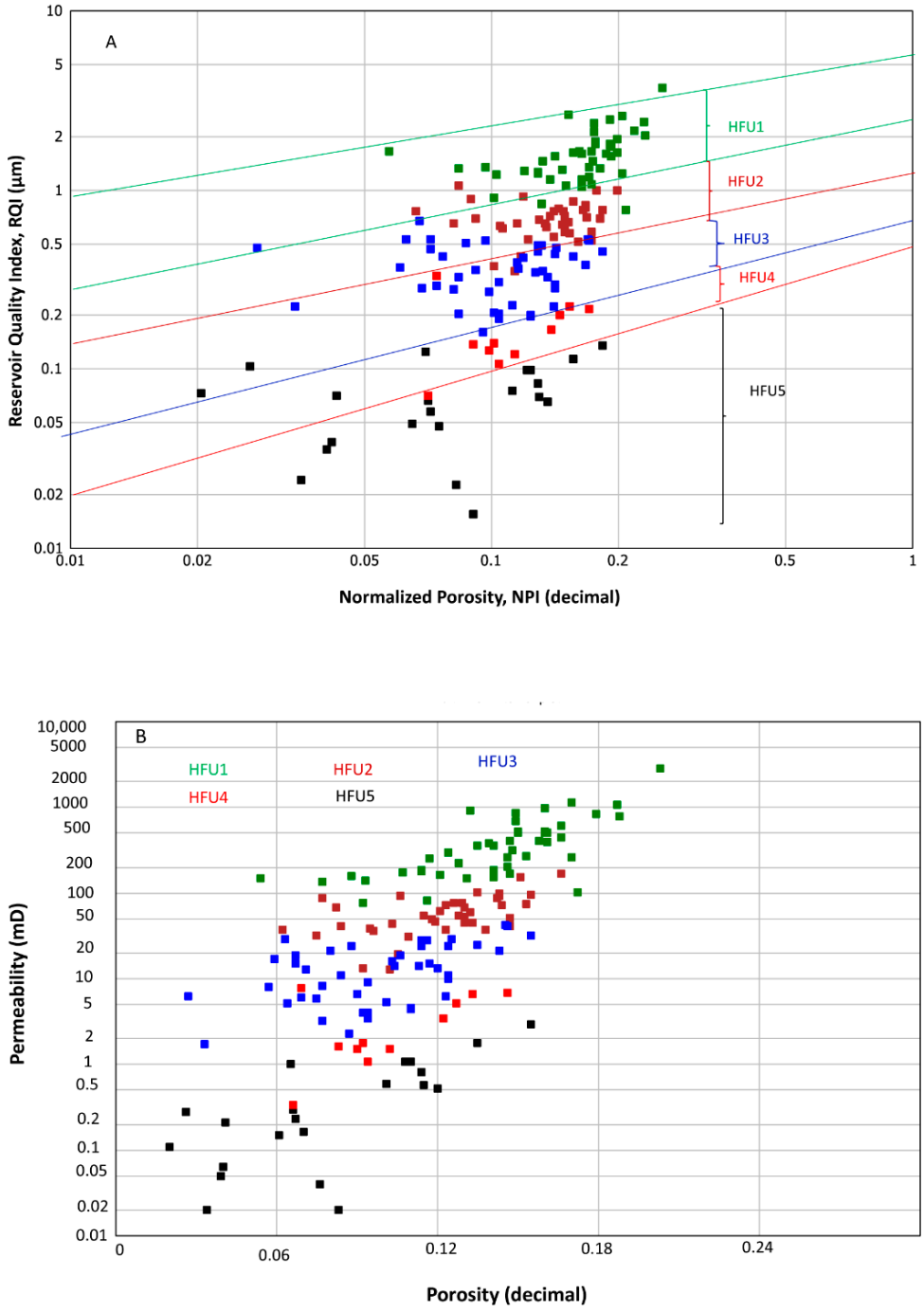

Figure 4. (**A**) Calculated FZI used to identify different HFUs from RQI versus NPI. (**B**) Permeability versus porosity plot showing different hydraulic flow units, HFU 1–5.

Based on the differences between the HFUs, it was concluded that HFU1 had the best reservoir quality, while HFU5 is classified as poor quality. The combination of the calculated Windland r35 and FZI petrophysical rock type zonation methods culminated in five different flow zones grouped as High (PRT1), Moderate (PRT2), Low (PRT3), Very low (PRT4), and Tight (PRT5) zones (Table 1). To estimate the storage and flow capacities in the flow zones, the SMLP method is performed.

4.2.3. SMLP

To understand the storage and flow capacities of and the petrophysical behaviour of the HFUs, and PRTs that make up a flow zone within a reservoir, the Stratigraphy-Modified Lorenz Plot (SMLP) method was applied in the studied wells. The SMLP method is based on porosity and permeability core data, multiplied by their respective bed thicknesses, normalized. The results produced the cumulative storage capacity (porosity multiplied by the bed thickness) and cumulative flow capacity (permeability multiplied by bed thickness). The cumulative flow capacity is plotted on the vertical axis against the cumulative storage capacity on the horizontal axis to produce a graph used to estimate storage and flow capacities [43,50,51]. Line segments and slopes of the graph separated by an inflexion point are used to represent flow and storage capacities. The steeper the slope represents the higher flow capacity, whereas the flattened slope represents a barrier or has insignificant flow capacity [47].

In this study, five different flow units, FU1-5 for well MO7, FU1-3 for well MO8 and FU1-5 in well MO9, are identified in Figure 5 and Table 2. The best flow units identified for individual wells are FU2 for well MO7, which contributes 28% and 50% storage and flow capacities, and FU1 in well MO8 (16% storage and 51% flow capacities) and MO9 (14% and 44% storage and flow capacities). At the same time, a minor contributor to storage and flow capacities is FU5, identified in well MO7 (13% and 1% storage and flow capacities) and MO9 (6% and 1% storage and flow capacities).

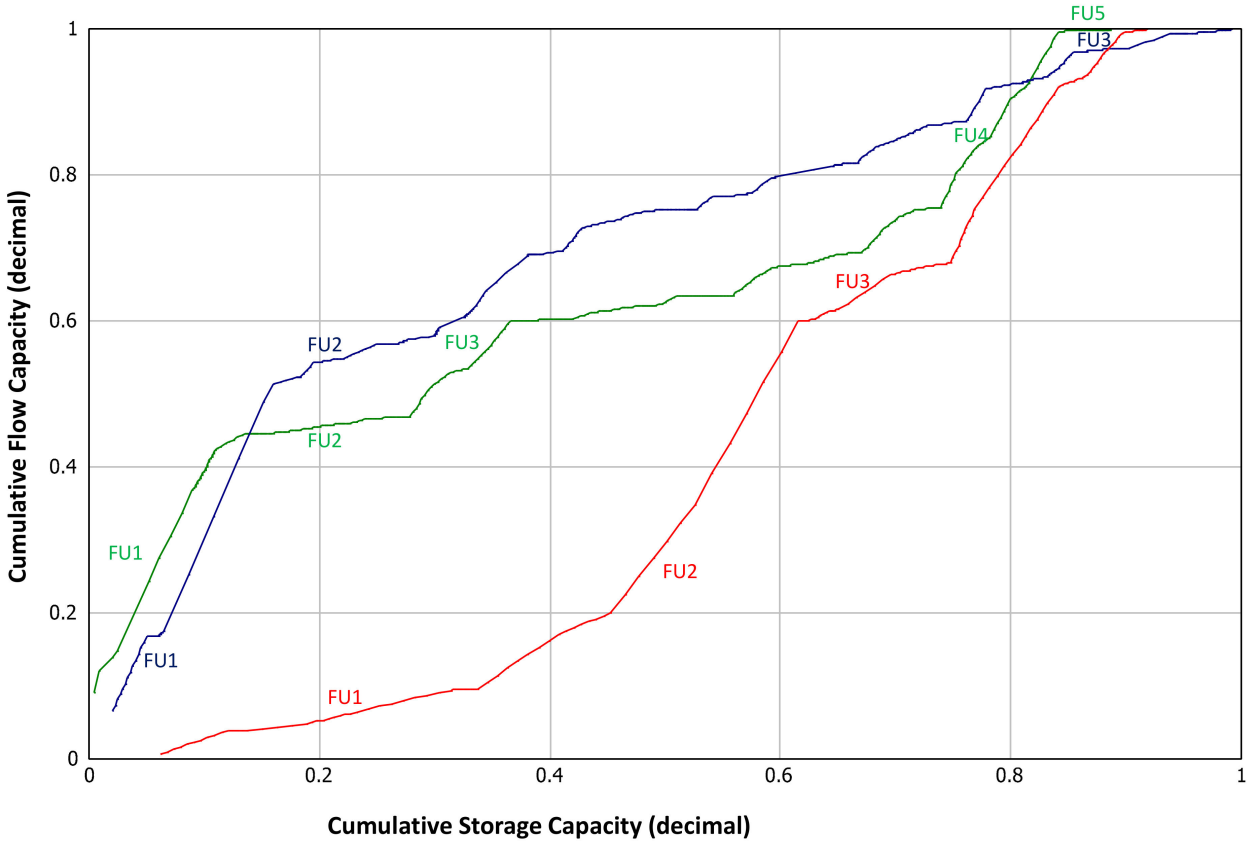

Figure 5. Plot of cumulative flow and storage capacities for wells showing five different flow units, FU1-5.

4.2.4. Identification of Flow Zones

The flow zones in the reservoirs of the studied wells were deciphered from the Winland r35 and FZI, calculated from the core-based porosity and permeability measurements and the mean values used to identify flow zones. Five flow zones identified in well MO7 as very low (2415–2418 m), moderate (2418–2429.3 m), low (2429.3–2435.7 m), moderate

(2435.7–2443.3 m) and tight (2443.3–2446.6 m) presented in Figure 6. The very low and moderate flow zones at the top of the reservoir are associated with facies B. Below the moderate zone is facies C, which is very fine to fine and very glauconitic, that separates the moderate and low zones. The low flow zone at depth sandwiched between the moderate zones serves as sand-to-sand contact that allows the flow of fluids between the moderate zones. Finally, the tight flow zone shows the lowest reservoir quality at the base of the reservoir. In terms of the storage and flow capacities, the very low flow zone contributed about 34% and 10% to storage and flow capacities.

Table 2. Storage and flow capacities estimated for wells.

	MO7		MO8		MO9	
FLOW UNIT	**Storage Capacity (%)**	**Flow Capacity (%)**	**Storage Capacity (%)**	**Flow Capacity (%)**	**Storage Capacity (%)**	**Flow Capacity (%)**
1	34.0	9.5	16.0	51.0	14.0	44.0
2	28.0	50.5	70.0	45.0	14.0	3.0
3	10.0	8.0	14.0	4.0	9.0	13.0
4	15.0	31.0	-	-	47.0	39.0
5	13.0	1.0	-	-	6.0	1.0

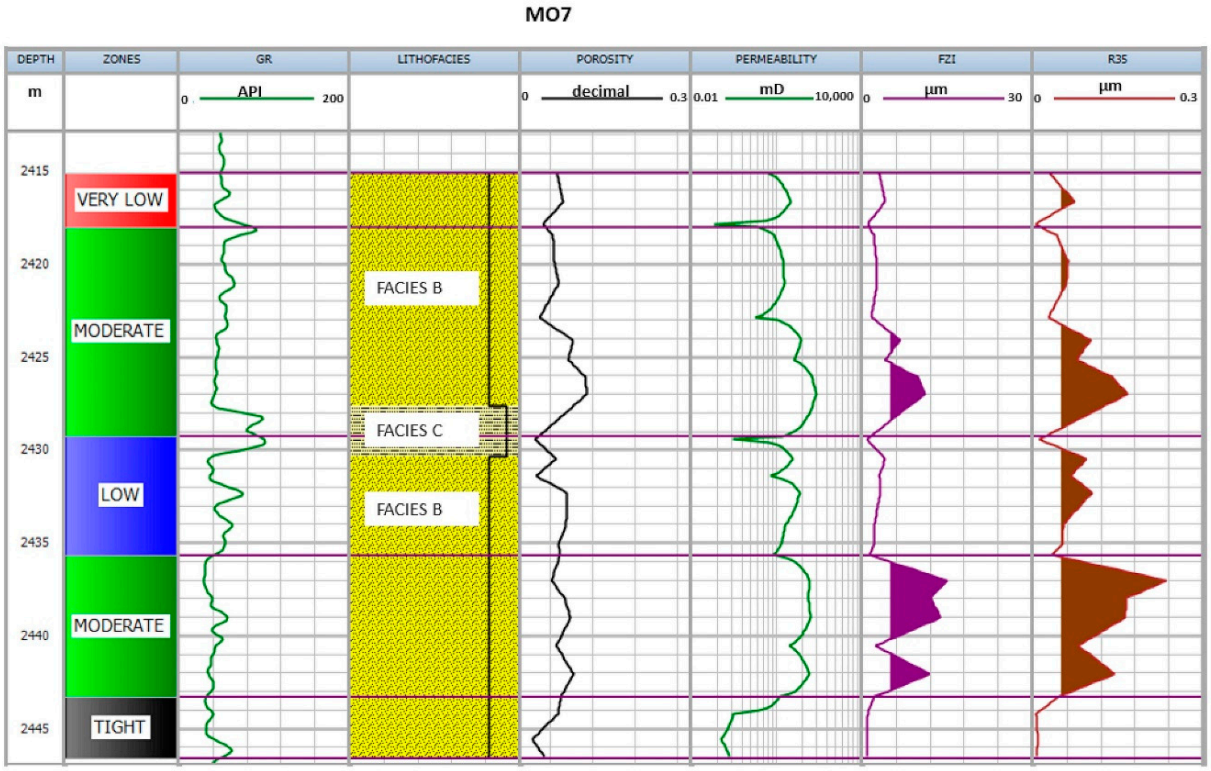

Figure 6. Results of well MO7 showing flow zones in track 2, gamma ray log in track 3, facies in track 4, porosity in track 5, permeability in track 6, FZI in track 7 and r35 in track 8.

In comparison, the moderate flow zone below the very low zone contributes 28% and 51% of storage and flow capacities. The combination of the low and moderate flow zones contributes 25% and 39% to storage and flow capacities. The tight flow zone has 13% storage capacity but 1% flow capacity. The upper moderate zone at depth 2418–2429.3 m is the most productive zone with a thickness of 31 m, an average porosity and permeability values of 7.8% and 30 mD.

Three distinct flow zones were identified for well MO7 as High (2368.2–2380.1 m), moderate zones (2380.1–2436.8 m), and Low zone (2436.8–2445.2 m), presented in Figure 7. Two lithofacies were identified as facies A and B associated with the high flow zone and

facies B with the moderate and the low flow zones. The high flow zone is the best reservoir quality with a 12 m average porosity of 14%, the permeability of 237 mD, r35 of 27 µm, FZI of 11.6 µm and 16% and 51% storage and flow capacities. Therefore, the reservoir quality recorded in well MO7 may be due to the dominance of facies A and B in this well. However, the reservoir quality tends to decline generally from the top of the reservoir to the bottom, with the low flow zone located at the bottom of the well.

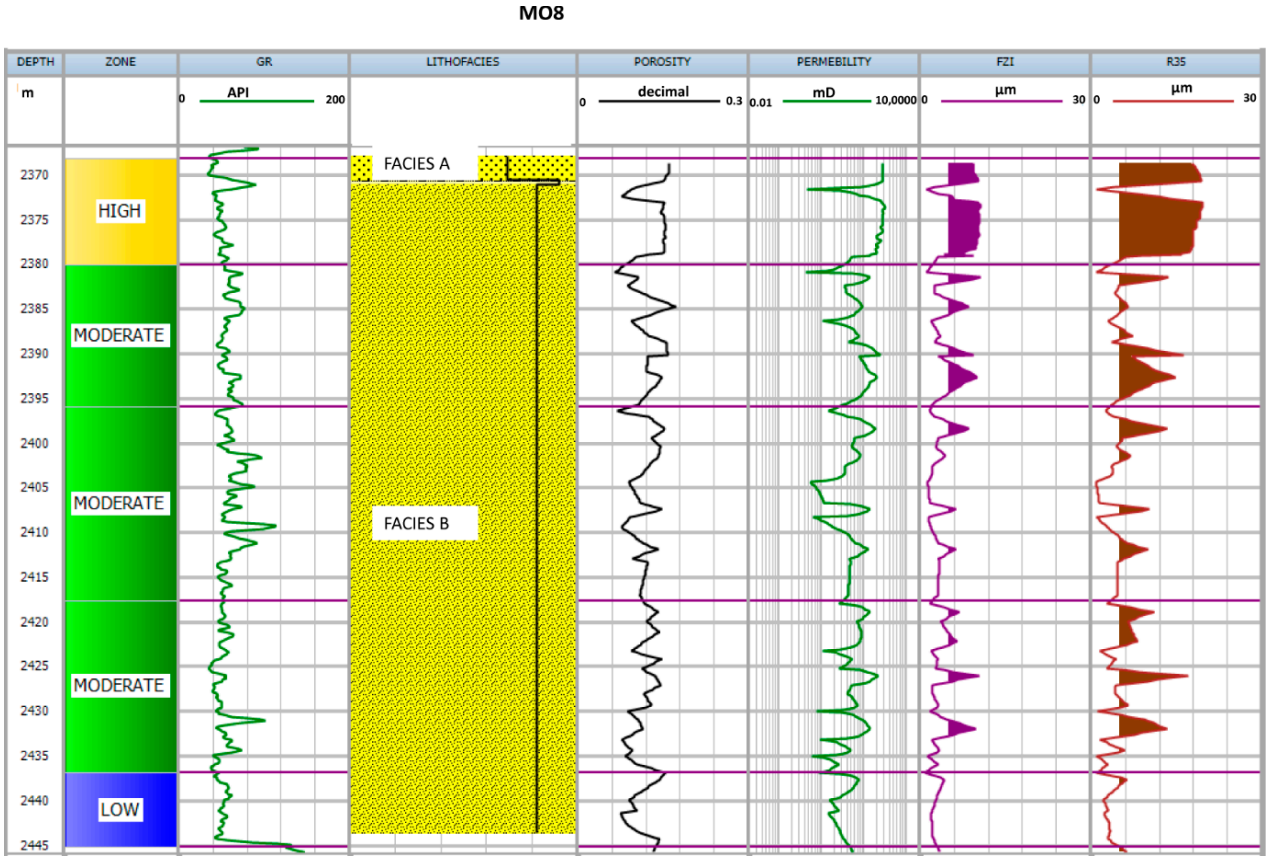

Figure 7. Results of well MO8 showing flow zones in track 2, gamma ray log in track 3, facies in track 4, porosity in track 5, permeability in track 6, FZI in track 7 and r35 in track 8.

Six flow zones were identified in well MO9 (Figure 8). At the top of the reservoir is the high flow zone (2369.2–2376.2 m), Low (2376.2–2387.2 m), High (2387.3–2393.3 m), Moderate (2387.3–2419.3 m), High (2419.3–2428.2 m) and Tight (2428.2–2442.4 m) at the bottom of the reservoir. The high flow zones are generally associated with facies A. The high flow zone at the top of the reservoir is the best. It contributes 14% and 44% to storage and flow capacities, while the combinations of the other two high flow zones, the low zone and the moderate zone, contribute 70% and 55% to storage and flow capacities. Conversely, the tight flow zone interpreted as the lowest rock quality is associated with facies D, mainly silt and claystone ranked as an impervious reservoir rock type with 6% storage and 1% flow capacities.

Flow zones are correlated to determine the lateral extent of the flow zones, as illustrated in Figure 9. Comparing flow zones between the studied wells indicates that the low and moderate flow zones are common to all the studied wells. The High productive flow zone identified at the upper reservoir in well MO8 was laterally traceable in well MO9. It is absent in well MO7 and probably has been truncated due to erosion. The high flow zone is about 12 m thick in well MO8 and thin (7 m) in well MO9, composed of FU1 (Table 2), which showed a storage capacity of 16% in well MO8 and 14% in well MO9, and flow capacity of 51% in well MO8 and 44% in well MO9. The very good petrophysical characteristics of the high flow zone indicate that significant quantities of gas can be produced from it, which

is comparable to a high flow zone identified in well PA1 at the central Bredasdorp Basin reported by [23].

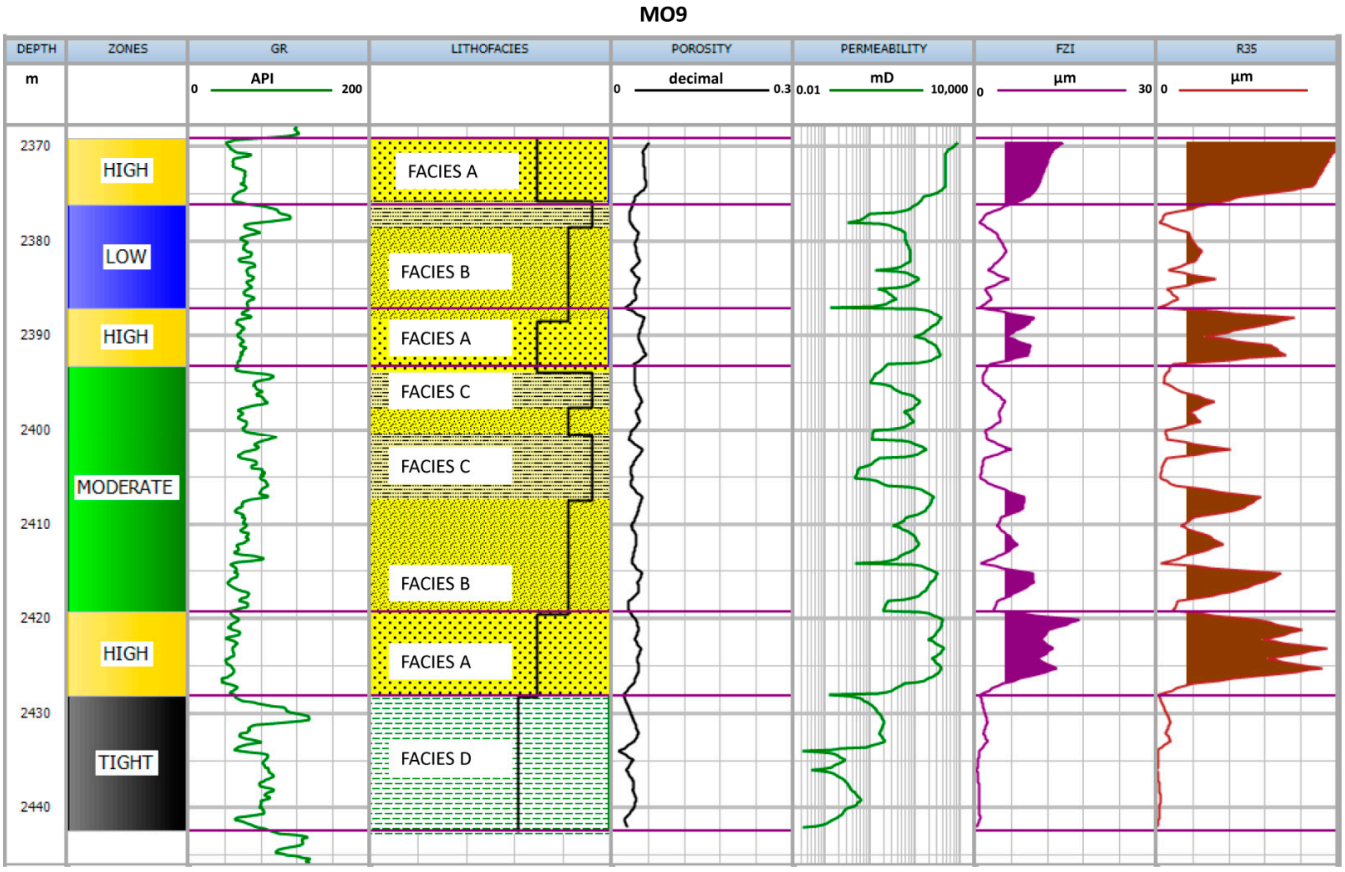

Figure 8. Results of well MO9 showing flow zones in track 2, gamma ray log in track 3, facies in track 4, porosity in track 5, permeability in track 6, FZI in track 7, and r35 in track 8.

Another productive zone identified is the moderate flow zone with a combined thickness of 56.7 m at well MO8 decreases in thickness as we move from well MO8 in the western part of the study area to 26 m and 31 m in well MO9 and MO7, respectively. Generally, the variations of the flow zones are interpreted to be controlled by combination facies and possibly diagenetic factors based on the closed association of the best facies associated with the best flow zones. The petrography results from XRD and SEM will now be integrated with the flow zones to establish the impacts of mineral compositions on flow zones.

4.2.5. Impacts of Mineral on Flow Zones

The quantitative results from XRD show that the mineral composition of the four samples from different flow zones (High, Moderate, Low, and Tight) is dominated by quartz and plagioclase (Table 3). The quartz content varies from 75.8% to 95.3%, while plagioclase ranges from 2.6% to 12.1%. The low and tight flow zones observed carbonate fragments of dolomite (7.5%) and calcite (8.5%). Muscovite varies from 0.4% in the high flow zone sample to 1.3% in the tight flow zone sample, while the highest microcline of 2.4% was recorded in the moderate and low flow zones, and 1.5% and 1.7% in the tight and high flow zones. In addition, the samples recorded low pyrite and kaolinite content. The impact of minerals on flow zones is evident as the plagioclase and muscovite content increases. An accompanied decrease in quartz content is observed, which implies that low plagioclase content of $\leq$4% and muscovite content of $\leq$1% corresponds to the low, moderate, and high flow zones, while plagioclase content of $\geq$4% and muscovite content of $\geq$1% belong to the

tight flow zone. Consequently, the quantity of plagioclase and muscovite can be used as a proxy to identify better reservoir quality rocks.

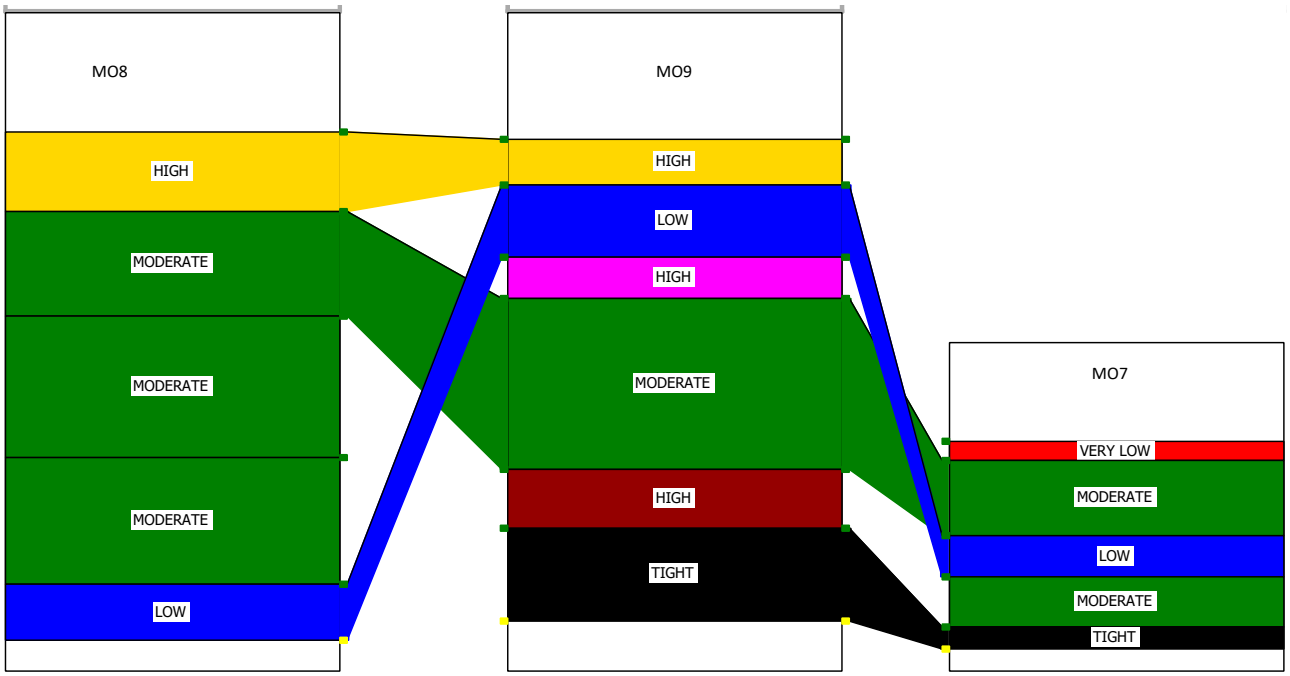

Figure 9. Correlation panel of flow zones showing lateral extension of the moderate and low flow zones in all the wells. The top high flow zone of well MO8 extends to well MO9 and truncated in well MO7 which may be due to erosion.

Table 3. Quantitative XRD results showing the mineral content of different minerals.

Well	Depth (m)	Zone Name	Quartz (%)	Dolomite (%)	Plagioclase (%)	Muscovite (%)	Calcite (%)	Microcline (%)	Pyrite (%)	Kaolinite (%)
MO7	2427	Moderate	93.7	0	3.2	0.6	0	2.4	0	0.1
MO7	2430	Low	84.6	7.5	3.8	1.4	0	2.4	0.2	0.2
MO9	2369	High	95.3	0	2.6	0.4	0	1.5	0	0.1
MO9	2442	Tight	75.8	0	12.1	1.3	8.5	1.7	0	0.7

The scanning electron microscopy results of morphological studies of four flow zones (high, moderate, low and tight) help in describing the pores and grain fabrics by imaging clay distributions and dominant pore and clay types (Figure 10A–D) because the quantitative XRD results cannot show the distribution and types of minerals in the pore spaces. The SEM analysis reveals that samples a–c in Figure 10 are composed of detrital constituents, cement and pores, while sample d is an illitic claystone with ragged illite plates with a few lath-shaped overgrowths (Figure 10). The significant detrital found in most of the samples is quartz. Monocrystalline detrital quartz is dominant and polycrystalline quartz is less abundant. The quartz grains are sub-angular to sub-rounded, with the monocrystalline grains, medium- to fine-grained, while the polycrystalline grains are medium- to coarse-grained, which shows information about the metamorphic source. This analysis also shows that there is slight alteration and the occurrence of a fracture. Intergranular porosity is visible, with samples a–c being more porous than sample d as it has less connectivity.

The reservoir quality enhancing factors include fracturing, dissolution and leaching [8,38,52,53]. For the different reservoir flow zones, the diagenetic process that reduces the rock quality can be attributed to quartz overgrowth and the accumulation of mica flakes in the pore spaces. In contrast, the fracture in Figure 10C, the high flow zone,

is interpreted as the reservoir quality enhancing process. The flow zones are generally controlled by a combination of facies and diagenetic factors.

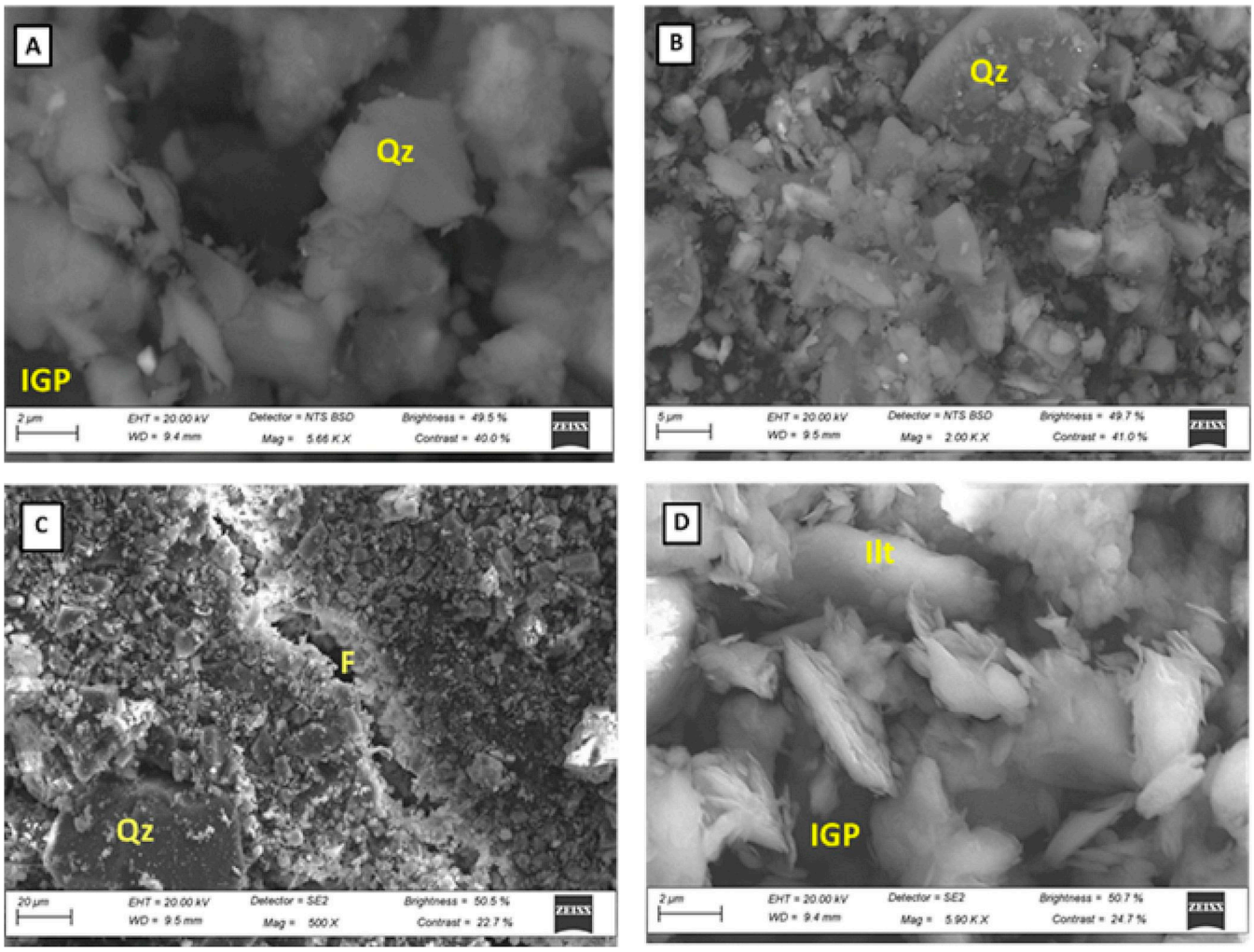

Figure 10. Scanning Electron Microscope (SEM) images: (**A**) Well MO7, 2427 m, intergranular pores (IGP) in slightly altered quartz (Qz) grains; (**B**) Well MO7, 2430 m, Finer grains of monocrystalline quartz derived from the coarser polycrystalline quartz (Qz) grains; (**C**) Well MO9, 2369 m, authigenic quartz (Qz), intergranular fracture (F) within finer quartz grains; (**D**) Well MO9, 2441 m, intergranular porosity (IGP) within plated illite (Ilt) grains.

5. Conclusions

In this study, the impact of detrital minerals in the sandstone reservoirs, northeastern Bredasdorp Basin, offshore of South Africa, have been investigated:

1. The lithofacies are interpreted as facies A, B, C and D based on the geological framework and five flow zones interpreted as high, moderate, low, very low and tight based on flow zone calculations.
2. The High productive flow zone identified at the upper reservoir in well MO8 was laterally traceable in well MO9. It is absent in well MO7 and probably has been truncated due to erosion. The high flow zone showed a storage capacity of 16% in well MO8 and 14% in well MO9 and a flow capacity of 51% in well MO8 and 44% in well MO9.
3. The very good petrophysical characteristics of the high flow zone indicate that significant quantities of gas can be produced from it, which is comparable to a high flow zone identified in well PA1 at the central Bredasdorp Basin.

4. The diagenetic process that reduces the rock quality can be attributed to quartz overgrowth, accumulation of mica flakes in the pore spaces and high content of plagioclase and muscovite.
5. Fracture observed in the high flow zone is interpreted as the reservoir quality enhancing process. The flow zones are generally controlled by a combination of facies and diagenetic factors.
6. This study has opened a door for researchers to investigate the vertical and lateral extent of the flow zone that extends to all wells studied.

Author Contributions: Conceptualization, M.O.; methodology, M.O., M.O.U., S.J. and M.M.; software, M.O. and M.M.; validation, M.O., M.O.U. and S.J.; formal analysis, M.O., M.O.U., S.J. and M.M.; writing—original draft preparation, M.O.; writing—review and editing, M.O., M.O.U., S.J. and M.M. All authors have read and agreed to the published version of the manuscript.

Funding: This research received no external funding.

Data Availability Statement: Not applicable.

Acknowledgments: The authors are grateful to the Petroleum Agency of South Africa for the provision of the dataset used in this study. Additionally, we are also thankful to LR-Senergy Company the United Kingdom for the provision of IP 4.7 software used for the petrophysical modelling.

Conflicts of Interest: The authors declare no conflict of interest.

References

1. Radwan, A.E.; Nabawy, B.S.; Kassem, A.A.; Hussein, W.S. Implementation of Rock Typing on Waterflooding Process during Secondary Recovery in Oil Reservoirs: A Case Study, El Morgan Oil Field, Gulf of Suez, Egypt. *Nat. Resour. Res.* **2021**, *30*, 1667–1696. [CrossRef]
2. Kassab, M.A.; Hashish, M.F.A.; Nabawy, B.S.; Elnaggar, O.M. Effect of Kaolinite as a Key Factor Controlling the Petrophysical Properties of the Nubia Sandstone in Central Eastern Desert, Egypt. *J. Afr. Earth Sci.* **2017**, *125*, 103–117. [CrossRef]
3. Magoba, M.; Opuwari, M. Petrophysical Interpretation and Fluid Substitution Modelling of the Upper Shallow Marine Sandstone Reservoirs in the Bredasdorp Basin, Offshore South Africa. *J. Pet. Explor. Prod. Technol.* **2020**, *10*, 783–803. [CrossRef]
4. Opuwari, M.; Kaushalendra, B.T.; Momoh, A. Sandstone Reservoir Zonation Using Conventional Core Data: A Case Study of Lower Cretaceous Sandstones, Orange Basin, South Africa. *J. Afr. Earth Sci.* **2019**, *153*, 54–66. [CrossRef]
5. Li, Y.; Chen, J.-Q.; Yang, J.-H.; Liu, J.-S.; Tong, W.-S. Determination of Shale Macroscale Modulus Based on Microscale Measurement: A Case Study Concerning Multiscale Mechanical Characteristics. *Pet. Sci.* **2022**, *19*, 1262–1275. [CrossRef]
6. Li, Y.; Chen, J.; Elsworth, D.; Pan, Z.; Ma, X. Nanoscale Mechanical Property Variations Concerning Mineral Composition and Contact of Marine Shale. *Geosci. Front.* **2022**, *13*, 101405. [CrossRef]
7. Ayodele, O.L.; Chatterjee, T.K.; Opuwari, M. Static Reservoir Modeling Using Stochastic Method: A Case Study of the Cretaceous Sequence of Gamtoos Basin, Offshore, South Africa. *J. Pet. Explor. Prod. Technol.* **2021**, *11*, 4185–4200. [CrossRef]
8. Nabawy, B.S.; Elgendy, N.T.; Gazia, M.T. Mineralogic and Diagenetic Controls on Reservoir Quality of Paleozoic Sandstones, Gebel El-Zeit, North Eastern Desert, Egypt. *Nat. Resour. Res.* **2020**, *29*, 1215–1238. [CrossRef]
9. Mode, A.W.; Anyiam, O.A.; Onwuchekwa, C.N. Flow Unit Characterization: Key to Delineating Reservoir Performance in "Aqua-Field", Niger Delta, Nigeria. *J. Geol. Soc. India* **2014**, *84*, 701–708. [CrossRef]
10. Wang, W.; Jiang, Y.; Swennen, R.; Yuan, J.; Liu, J.; Zhang, S. Pore-Throat Characteristics of Tight Sandstone Reservoirs Composed of Gravity Flow Sediments: Yingcheng Formation, Longfengshan Sag, China. *J. Pet. Sci. Eng.* **2018**, *171*, 646–661. [CrossRef]
11. Opuwari, M. An Integrated Approach of Fluid Contact Determination of the Albian Age Sandstone Reservoirs of the Orange Basin Offshore South Africa. *Mar. Georesour. Geotechnol.* **2021**, *39*, 876–888. [CrossRef]
12. Mohammadian, E.; Kheirollahi, M.; Liu, B.; Ostadhassan, M.; Sabet, M. A Case Study of Petrophysical Rock Typing and Permeability Prediction Using Machine Learning in a Heterogenous Carbonate Reservoir in Iran. *Sci. Rep.* **2022**, *12*, 4505. [CrossRef] [PubMed]
13. Opuwari, M.; Amponsah-Dacosta, M.; Mohammed, S.; Egesi, N. Delineation of Sandstone Reservoirs of Pletmos Basin Offshore South Africa into Flow Units Using Core Data. *S. Afr. J. Geol.* **2020**, *123*, 479–492. [CrossRef]
14. Nabawy, B.S. An Improved Stratigraphic Modified Lorenz (ISML) Plot as a Tool for Describing Efficiency of the Hydraulic Flow Units (HFUs) in Clastic and Non-Clastic Reservoir Sequences. *Geomech. Geophys. Geo-Energy Geo-Resour.* **2021**, *7*, 67. [CrossRef]
15. Dar, Q.U.; Pu, R.; Baiyegunhi, C.; Shabeer, G.; Ali, R.I.; Ashraf, U.; Sajid, Z.; Mehmood, M. The Impact of Diagenesis on the Reservoir Quality of the Early Cretaceous Lower Goru Sandstones in the Lower Indus Basin, Pakistan. *J. Pet. Explor. Prod. Technol.* **2022**, *12*, 1437–1452. [CrossRef]
16. Leila, M.; Moscariello, A.; Šegvić, B. Depositional Facies Controls on the Diagenesis and Reservoir Quality of the Messinian Qawasim and Abu Madi Formations, Onshore Nile Delta, Egypt. *Geol. J.* **2019**, *54*, 1797–1813. [CrossRef]

17. Li, Y.; Gao, X.; Meng, S.; Wu, P.; Niu, X.; Qiao, P.; Elsworth, D. Diagenetic Sequences of Continuously Deposited Tight Sandstones in Various Environments: A Case Study from Upper Paleozoic Sandstones in the Linxing Area, Eastern Ordos Basin, China. *AAPG Bulletin* **2019**, *103*, 2757–2783. [CrossRef]
18. Li, Y.; Wang, Z.; Pan, Z.; Niu, X.; Yu, Y.; Meng, S. Pore Structure and Its Fractal Dimensions of Transitional Shale: A Cross-Section from East Margin of the Ordos Basin, China. *Fuel* **2019**, *241*, 417–431. [CrossRef]
19. Ayodele, O.L.; van Bever Donker, J.M.; Opuwari, M. Pore Pressure Prediction of Some Selected Wells from the Southern Pletmos Basin, Offshore South Africa. *S. Afr. J. Geol.* **2016**, *119*, 203–214. [CrossRef]
20. Ramiah, K.; Trivedi, K.B.; Opuwari, M. A 2D Geomechanical Model of an Offshore Gas Field in the Bredasdorp Basin, South Africa. *J. Pet. Explor. Prod. Technol.* **2019**, *9*, 207–222. [CrossRef]
21. Zhang, Z.; Zhang, H.; Li, J.; Cai, Z. Permeability and Porosity Prediction Using Logging Data in a Heterogeneous Dolomite Reservoir: An Integrated Approach. *J. Nat. Gas Sci. Eng.* **2021**, *86*, 103743. [CrossRef]
22. Ali, M.; Abdelhady, A.; Abdelmaksoud, A.; Darwish, M.; Essa, M.A. 3D Static Modeling and Petrographic Aspects of the Albian/Cenomanian Reservoir, Komombo Basin, Upper Egypt. *Nat. Resour. Res.* **2020**, *29*, 1259–1281. [CrossRef]
23. Opuwari, M.; Dominick, N. Sandstone Reservoir Zonation of the North-Western Bredasdorp Basin South Africa Using Core Data. *J. Appl. Geophys.* **2021**, *193*, 104425. [CrossRef]
24. Opuwari, M.; Mohammed, S.; Ile, C. Determination of Reservoir Flow Units from Core Data: A Case Study of the Lower Cretaceous Sandstone Reservoirs, Western Bredasdorp Basin Offshore in South Africa. *Nat. Resour. Res.* **2021**, *30*, 411–430. [CrossRef]
25. Opuwari, M.; Afolayan, B.; Mohammed, S.; Amaechi, P.O.; Bareja, Y.; Chatterjee, T. Petrophysical Core-Based Zonation of OW Oilfield in the Bredasdorp Basin South Africa. *Sci. Rep.* **2022**, *12*, 510. [CrossRef]
26. McMillan, I.K.; Brink, G.I.; Broad, D.S.; Maier, J.J. Late Mesozoic Sedimentary Basins off the South Coast of South Africa. In *Sedimentary Basins of the World*; Elsevier: Amsterdam, The Netherlands, 1997; Volume 3, pp. 319–376.
27. Jungslager, E.H. Petroleum Habitats of the Atlantic Margin of South Africa. *Geol. Soc. Lond. Spec. Publ.* **1999**, *153*, 153–168. [CrossRef]
28. Petroleum Agency of South Africa. Petroleum Agency of South Africa. Petroleum Exploration Information and Opportunities. In *Petroleum Agency South Africa Report*; Petroleum Agency of South Africa: Cape Town, South Africa, 2003.
29. Saffou, E.; Raza, A.; Gholami, R.; Croukamp, L.; Elingou, W.R.; van Bever Donker, J.; Opuwari, M.; Manzi, M.S.; Durrheim, R.J. Geomechanical Characterization of CO2 Storage Sites: A Case Study from a Nearly Depleted Gas Field in the Bredasdorp Basin, South Africa. *J. Nat. Gas Sci. Eng.* **2020**, *81*, 103446. [CrossRef]
30. Brown, L.F. *Sequence Stratigraphy in Offshore South African Divergent Basins: An Atlas on Exploration for Cretaceous Lowstand Traps by Soekor (Pty) Ltd, AAPG Studies in Geology 41*; AAPG: Tulsa, OK, USA, 1995.
31. Broad, D.S.; Jungslager, E.H.A.; McLachlan, I.R.; Roux, J. Offshore Mesozoic Basins. *Geol. S. Afr. Geol. Soc. S. Afr. Johannesbg./Counc. Geosci. Pretoria* **2006**, *553*, 571.
32. Paton, D.A.; Di Primio, R.; Kuhlmann, G.; Van Der Spuy, D.; Horsfield, B. Insights into the Petroleum System Evolution of the Southern Orange Basin, South Africa. *S. Afr. J. Geol.* **2007**, *110*, 261–274. [CrossRef]
33. Masindi, R.; Trivedi, K.B.; Opuwari, M. An Integrated Approach of Reservoir Characterization of Y Gas Field in Central Bredasdorp Basin, South Africa. *J. Pet. Explor. Prod. Technol.* **2022**, 1–19. [CrossRef]
34. Burden, P.L.; Davies, C.P. South Africa Offshore EXP. II: Oribi Field Is South Africa's First Offshore Crude Oil Production. *Oil Gas J.* **1997**, *95*, 63–65.
35. Winland, H.D. Amoco Production Research Report No. F72-G25 1972. In *Oil Accumulation in Response to Pore Size Changes, Weyburn Field, Saskatchewan*; Amoco: London, UK, 1972.
36. Amaefule, J.O.; Altunbay, M.; Tiab, D.; Kersey, D.G.; Keelan, D.K. Enhanced Reservoir Description: Using Core and Log Data to Identify Hydraulic (Flow) Units and Predict Permeability in Uncored Intervals/Wells. In Proceedings of the SPE Annual Technical Conference and Exhibition, Houston, TX, USA, 3–6 October 1993.
37. Porras, J.C.; Barbato, R.; Khazen, L. Reservoir Flow Units: A Comparison between Three Different Models in the Santa Barbara and Pirital Fields, North Monagas Area, Eastern Venezuela Basin. In Proceedings of the Latin American and Caribbean Petroleum Engineering Conference, Caracas, Venezuela, 21 April 1999.
38. Fea, I.; Abioui, M.; Nabawy, B.S.; Jain, S.; Bruno, D.Z.; Kassem, A.A.; Benssaou, M. Reservoir Quality Discrimination of the Albian-Cenomanian Reservoir Sequences in the Ivorian Basin: A Lithological and Petrophysical Study. *Geomech. Geophys. Geo-Energy Geo-Resour.* **2022**, *8*, 1. [CrossRef]
39. El Sharawy, M.S.; Nabawy, B.S. Integration of Electrofacies and Hydraulic Flow Units to Delineate Reservoir Quality in Uncored Reservoirs: A Case Study, Nubia Sandstone Reservoir, Gulf of Suez, Egypt. *Nat. Resour. Res.* **2019**, *28*, 1587–1608. [CrossRef]
40. Adegbite, J.O.; Belhaj, H.; Bera, A. Investigations on the Relationship among the Porosity, Permeability and Pore Throat Size of Transition Zone Samples in Carbonate Reservoirs Using Multiple Regression Analysis, Artificial Neural Network and Adaptive Neuro-Fuzzy Interface System. *Pet. Res.* **2021**, *6*, 321–332. [CrossRef]
41. Khalid, M.; Desouky, S.E.-D.; Rashed, M.; Shazly, T.; Sediek, K. Application of Hydraulic Flow Units' Approach for Improving Reservoir Characterization and Predicting Permeability. *J. Pet. Explor. Prod. Technol.* **2020**, *10*, 467–479. [CrossRef]
42. Kolodzie, S. Analysis of Pore Throat Size and Use of the Waxman-Smits Equation to Determine OOIP in Spindle Field, Colorado. In Proceedings of the SPE Annual Technical Conference and Exhibition, Dallas, TX, USA, 21 September 1980.

43. Gunter, G.W.; Finneran, J.M.; Hartmann, D.J.; Miller, J.D. Early Determination of Reservoir Flow Units Using an Integrated Petrophysical Method. In Proceedings of the SPE Annual Technical Conference and Exhibition, San Antonio, TX, USA, 5–8 October 1997.
44. Ebanks, W.J., Jr.; AAPG. *Flow Unit Concept-Integrated Approach to Reservoir Description for Engineering Projects*; AAPG: Tulsa, OK, USA, 1987; Volume 71.
45. Hearn, C.L.; Ebanks, W.J.; Tye, R.S.; Ranganathan, V. Geological Factors Influencing Reservoir Performance of the Hartzog Draw Field, Wyoming. *J. Pet. Technol.* **1984**, *36*, 1335–1344. [CrossRef]
46. Slatt, R.M.; Hopkins, G.L. Scaling Geologic Reservoir Description to Engineering Needs. *J. Pet. Technol.* **1990**, *42*, 202–210. [CrossRef]
47. Pranter, M.J.; Hurley, N.F.; Davis, T.L. *Sequence-Stratigraphic, Petrophysical, and Multicomponent Seismic Analysis of a Shelf-Margin Reservoir: San Andres Formation (Permian), Vacuum Field, New Mexico, United States*; ACS Publishers: Washington, DC, USA, 2004.
48. Guo, S.; Focke, W.W.; Tichapondwa, S.M. Sn/Mn/Bi2O3 Ternary Pyrotechnic Time Delay Compositions. *ACS Sustain. Chem. Eng.* **2020**, *8*, 14524–14530. [CrossRef]
49. Nabawy, B.S.; Al-Azazi, N.A. Reservoir Zonation and Discrimination Using the Routine Core Analyses Data: The Upper Jurassic Sab'atayn Sandstones as a Case Study, Sab'atayn Basin, Yemen. *Arab. J. Geosci.* **2015**, *8*, 5511–5530. [CrossRef]
50. Yu, P. Hydraulic Unit Classification of Un-Cored Intervals/Wells and Its Influence on the Productivity Performance. *J. Pet. Sci. Eng.* **2021**, *197*, 107980. [CrossRef]
51. Asadi, A.; Rahimpour-Bonab, H.; Aleali, M.; Arian, M. Geologically Based Integrated Approach for Zonation of a Late Jurassic–Early Cretaceous Carbonate Reservoir; a Case from Persian Gulf. *J. Pet. Explor. Prod. Technol.* **2022**, *12*, 1265–1283. [CrossRef]
52. Alqubalee, A.; Babalola, L.; Abdullatif, O.; Makkawi, M. Factors Controlling Reservoir Quality of a Paleozoic Tight Sandstone, Rub'al Khali Basin, Saudi Arabia. *Arab. J. Sci. Eng.* **2019**, *44*, 6489–6507. [CrossRef]
53. Makeen, Y.M.; Shan, X.; Lawal, M.; Ayinla, H.A.; Su, S.; Yelwa, N.A.; Liang, Y.; Ayuk, N.E.; Du, X. Reservoir Quality and Its Controlling Diagenetic Factors in the Bentiu Formation, Northeastern Muglad Basin, Sudan. *Sci. Rep.* **2021**, *11*, 18442. [CrossRef] [PubMed]